Satb1 regulates hematopoietic stem cell self-renewal by promoting quiescence and repressing differentiation commitment

Britta Will[1,2], **Thomas O. Vogler**[1], **Boris Bartholdy**[1], **Francine Garrett-Bakelman**[3], **Jillian Mayer**[1], **Laura Barreyro**[1], **Ashley Pandolfi**[1], **Tihomira I. Todorova**[1], **Ujunwa C. Okoye-Okafor**[1], **Robert F. Stanley**[1], **Tushar D. Bhagat**[4], **Amit Verma**[2,4,5,6], **Maria E. Figueroa**[7], **Ari Melnick**[3], **Michael Roth**[1], and **Ulrich Steidl**[1,2,5,6]

[1]Department of Cell Biology, Albert Einstein College of Medicine, Bronx, NY 10461

[2]Ruth L. and David S. Gottesman Institute for Stem Cell and Regenerative Medicine Research, Albert Einstein College of Medicine, Bronx, NY 10461

[3]Department of Medicine, Weill Cornell Medical College, New York, NY 10021

[4]Department of Developmental and Molecular Biology, Albert Einstein College of Medicine, Bronx, NY 10461

[5]Department of Medicine (Oncology), Albert Einstein College of Medicine, Bronx, NY 10461

[6]Albert Einstein Cancer Center, Albert Einstein College of Medicine, Bronx, NY 10461

[7]Department of Pathology, University of Michigan Medical School, Ann Arbor, MI 48109

Abstract

How hematopoietic stem cells coordinate the regulation of opposing cellular mechanisms like self-renewal and differentiation commitment remains unclear. Here, we identified the transcription factor and chromatin remodeler *Satb1* as a critical regulator of the hematopoietic stem cell (HSC) fate. HSCs lacking *Satb1* displayed defective self-renewal, less quiescence and accelerated lineage commitment, resulting in progressive depletion of functional HSCs. Increased commitment was caused by reduced symmetric self-renewal and increased symmetric differentiation divisions of Satb1-deficient HSCs. Satb1 simultaneously repressed gene sets involved in HSC activation and cellular polarity, including *Numb* and *Myc*, two key factors for stem cell fate specification. Thus, Satb1 is a regulator that promotes HSC quiescence and represses lineage commitment.

Corresponding author: Ulrich Steidl, Albert Einstein College of Medicine, Department of Cell Biology, Chanin Bldg. Rm. #606, 1300 Morris Park Avenue, Bronx, NY 10461, U.S.A. ulrich.steidl@einstein.yu.edu Tel: +1 718-430-3437 Fax: +1 718-430-8574 .

In metazoans, adult tissue-specific stem cells (SCs) constitute a rare population of long-lived cells possessing the ability to give rise to multiple differentiated cell types. Hematopoietic stem cells (HSCs) ensure the life-long generation of all cells of the innate and adaptive immune system, as well as red blood cells and platelets[1]. Like many other tissue-specific SCs in multicellular organisms, HSCs exhibit key features separating them functionally from differentiated cell types: relative cellular quiescence, self-maintenance and multilineage differentiation capacity[2, 3]. Balancing HSC self-renewal and differentiation is crucial for the long-term maintenance of the pool of functional HSCs and thus for their ability to sustain blood cell production and regeneration[4]. Alterations in the balance between quiescence and activation, self-renewal and differentiation are known to exhaust HSCs[5] or lead to their malignant transformation[6].

Transcriptional regulation by specific factors is critical to ensure the appropriate function of both embryonic and adult tissue-specific stem cells, in part by governing their ability to self-renew and differentiate[7]. The interplay of transcriptional programs, rather than individual transcription factors, determines the entire set of SC functions including fate decisions[8, 9]. However, how individual functions such as SC quiescence, division, and lineage commitment are coordinately regulated only begins to be understood. Global epigenetic regulation was shown to have an important role in the function and lineage differentiation of SCs including HSCs[8, 10, 11]. However, it is still largely unknown how specific epigenetic factors impact and integrate gene activation and repression of multiple transcriptional programs in SCs.

Satb1 (special AT-rich sequence-binding protein 1) was identified as a chromatin organizer that forms "cage-like" chromatin networks in the nucleus of T cell precursors, tethering together specific DNA sequences and regulating the expression of several genes relevant for T cell maturation[12-14]. Satb1 is also involved in the differentiation of other hematopoietic lineages[15] and embryonic stem cells by controlling expression of transcriptional master regulators, such as *Sfpi1*[15] or *Nanog*[16]. Several studies have also linked *Satb1* with cancer. Enhanced activity of this epigenetic factor is capable of reprogramming transcriptional networks and promoting aberrant growth and metastasis in different types of epithelial tumors[17-19]. Additionally, impairment of Satb1 is associated with a subtype of acute myelogenous leukemia[15]. The role of Satb1 in tissue-specific SCs including HSCs has not been examined thus far.

Here, we investigated the role of *Satb1* in HSCs and found that Satb1 critically mediates multiple, functionally linked HSC properties. *Satb1* is crucial for the maintenance of HSC self-renewal and exerts its function through simultaneously regulating transcriptional programs associated with the cell polarity factor *Numb, Myc* and several cell cycle regulators, thereby promoting quiescence and repressing lineage commitment in HSCs.

Results

Satb1 deficiency impairs long-term repopulation capacity of HSCs

To characterize *Satb1* mRNA and protein expression in immature hematopoietic cells we performed qRT-PCR and immunohistochemistry on purified murine HSCs (CD150+ Lin−

cKit$^+$ Sca-1$^+$ (LSK)), multipotent progenitor cells (MPPs; CD150$^-$ LSK), common myeloid progenitor cells (CMPs; CD34$^+$ FcγRII/III$^-$ cKit$^+$ Sca-1$^-$ Lin$^-$), granulocytic-monocytic progenitor cells (GMPs; CD34$^+$ FcγRII/III$^+$ cKit$^+$ Sca-1$^-$ Lin$^-$), and megakaryocytic-erythroid progenitor cells (MEPs; CD34$^-$ FcγRII/III$^-$ cKit$^+$ Sca-1$^-$ Lin$^-$) (for sorting strategy see Supplementary Fig. 1a). We found *Satb1* mRNA and protein to be highly expressed in thymocytes and well detectable in all bone marrow-derived stem and progenitor cells (Fig. 1a,b). Among the immature hematopoietic cell populations, Satb1 expression was highest in the HSC, MPP and CMP compartments, and decreased in lineage-restricted GMPs and MEPs. Satb1 was localized in the nucleus in HSCs as assessed by confocal microscopy (Fig. 1c). In thymocytes, Satb1 was reported in the nucleus and shown to act as a transcriptional regulator[20, 21].

To assess the role of *Satb1* in HSC function, we examined multilineage reconstitution and long-term self-maintenance capacities of HSCs utilizing a *Satb1*$^{-/-}$ mouse model in which the first five of eleven exons, encoding 213 amino acids including the translation start codon, were eliminated and result in a complete lack of Satb1 protein[12]. We first characterized fetal hematopoiesis, as homozygous *Satb1*$^{-/-}$ animals die around the time of birth. Flow cytometry analysis showed normal frequencies of HSCs, MPPs, CMPs, GMPs, and MEPs in the fetal liver at E17-18.5 days (Supplementary Fig. 1b). Colony assays revealed that compared to wild-type cells, *Satb1*$^{-/-}$ fetal livers contain a significantly increased number of functional colony-initiating progenitors of the granulocytic-monocytic (2.2 ± 0.6-fold), erythroid (4.3 ± 1.9-fold) and monocytic lineages (15.5 ± 7.1-fold) (Supplementary Fig. 1c). Non-competitive transplantation of *Satb1*$^{-/-}$ and wild-type fetal liver cells resulted in comparable hematopoietic reconstitution 24 weeks after transplantation (Supplementary Fig. 1d) with no significant effect on the reconstitution of mature myeloid, erythroid, or B cells (Fig. 1d,e); only the CD4$^+$ T cells were moderately reduced which is consistent with previous observations[12]. The frequency of functional HSCs in E17-18.5 fetal livers was also not found significantly changed by the absence of *Satb1*, as determined by competitive limiting dilution transplantation assays (Supplementary Fig. 1e). These findings show that during embryogenesis, *Satb1* is neither essential for the generation of HSCs, nor for their short-term multi-lineage repopulation capacity.

In order to evaluate the long-term self-renewal ability of HSCs in the absence of *Satb1*, we conducted competitive serial transplantation experiments[22]. Unfractionated *Satb1*$^{-/-}$ cells from the fetal liver showed a progressive repopulation defect in serial competitive transplantations, with a $42 \pm 2.4\%$ reduction in the second reconstitution, $71.3 \pm 12.9\%$ reduction in third, and $91.3 \pm 2.7\%$ reduction in the fourth serial transfer in comparison to wild-type cells (Fig. 1f and Supplementary Fig. 2a). Serial transplantation of purified *Satb1*$^{-/-}$ HSCs also showed a progressive loss of repopulation capacity compared to wild-type HSCs, with a $44 \pm 15\%$ reduction in second and $69 \pm 25\%$ reduction in third serial transfer (Fig. 1g and Supplementary Fig. 2b). Characterization of the repopulation of different cell lineages showed a reconstitution impairment in all compartments (Supplementary Fig. 2c), indicative of a defect at the stem cell level. Taken together, these data show that *Satb1* is indispensable for long-term self-renewal of HSCs, and that the absence of *Satb1* leads to a progressive decrease of functional HSCs.

Satb1-deficient hematopoietic stem cells are less quiescent

The maintenance of a quiescent state is an important feature of HSCs and loss of quiescence has been shown to lead to the loss of functional HSCs[23]. To determine whether *Satb1* regulates HSC quiescence we compared the number of quiescent and actively cycling HSCs in wild-type or *Satb1*^{−/−} mice *in vivo* using Pyronin Y and Hoechst 33343 intercalation assays[24] on immature LSK (Lin[−] Sca-1^{+} cKit^{+}) cells (Fig. 2a,b) as well as on purified HSCs (Fig. 2c). In both stem cell-containing populations the number of quiescent cells in the G_0 phase of the cell cycle was significantly reduced in the absence of *Satb1* (Fig. 2b,c). However, most apparent differences in the cell cycle distribution were observed within the purified HSC population, in which $36 \pm 4.5\%$ of *Satb1*^{−/−} cells compared to $53.5 \pm 2.1\%$ wild-type HSC were found in G_0, while the number of *Satb1*^{−/−} HSC in G_1 (63 ± 5.7) was significantly increased compared to wild-type ($42.5 \pm 3.5\%$; Fig. 2c). Consistently, the alteration in cell cycle activity was accompanied by a change in cell division kinetics. When using individually sorted, highly enriched HSCs (CD150^{+} CD48^{−} LSK), significantly less *Satb1*^{−/−} HSCs ($5 \pm 2.4\%$) remained in an undivided state compared to wild-type HSCs ($20.7 \pm 3.4\%$), while significantly more *Satb1*^{−/−} HSCs divided once compared to wild-type ($77.5 \pm 1.2\%$ versus $61.5 \pm 1.2\%$) after 48hrs in an *ex vivo* culture assay (Fig. 2d). Consistently, we found that *Satb1* expression in wild-type HSCs is cell cycle phase-dependent, with highest *Satb1* expression in G_0 (Supplementary Fig. 2d). *Satb1* expression in HSCs decreased significantly upon HSC activation under stress conditions *in vivo* (5-fluorouracil treatment) (Supplementary Figure 2e). Together, these results indicate that *Satb1* promotes quiescence of HSCs under steady state as well as stress conditions.

Satb1-deficient HSC show increased differentiation commitment

To further elucidate functional alterations of adult *Satb1*^{−/−} HSCs we characterized the composition of hematopoietic stem and multipotent progenitor cell compartments following competitive congenic transplantation of wild-type and *Satb1*^{−/−} cells. Recipients of unfractionated *Satb1*^{−/−} fetal liver cells showed a significant reduction of HSCs (CD150^{+} CD48^{−} LSK) ($4.2 \pm 3.6\%$) compared to recipients of wild-type cells ($13.9 \pm 11.6\%$), and an increase of CD150^{−} CD48^{+} LSK multipotent progenitor cells ($77.5 \pm 12.9\%$ compared to $61.4 \pm 16.9\%$ in recipients of wild-type cells; Fig. 3a,b). Quantification of the number of HSCs (CD150^{+} CD48^{−} LSK) and MPPs (CD150^{−} CD48^{+} LSK) also showed a significant decrease of HSCs (46 ± 40 cells/10^6 compared to 107 ± 71 cells/10^6 total nucleated bone marrow cells) and a significant increase of MPPs (944 ± 446 cells/10^6 compared to 549 ± 254 cells/10^6 total nucleated bone marrow cells) in recipients of *Satb1*^{−/−} compared to recipients of wild-type cells (Fig. 3c).

To test if *Satb1*^{−/−} HSCs are more prone to commit to differentiation, we evaluated colony-formation capacities of fractionated CD150^{+} CD48^{−} LSK and CD150^{+} CD48^{+} LSK cells, and MPPs (CD150^{−}CD48^{+} LSK ; Fig. 3d-f). *Satb1*^{−/−} CD150^{+} CD48^{−} LSK cells formed 1.6-fold more erythroid burst colony forming units (BFU-E), 1.9-fold more granulocyte-monocyte colony forming units (CFU-GM), and 1.8-fold more granulocyte-erythrocyte-monocyte-megakaryocyte colony forming units (CFU-GEMM) compared to wild-type (Fig. 3d). Similarly, CD150^{+} CD48^{+} LSK cells also showed a 1.7-fold increase in the generation of CFU-GM, 1.8-fold increase in CFU-G or M, and a 1.6-fold increase in CFU-GEMM (Fig.

3e). This increased myeloid colony formation in *Satb1*−/− cells was restricted to the HSC compartments, as we did not observe a significant change in the colony formation of MPPs (Fig. 3f). These findings suggest that Satb1 suppresses differentiation commitment specifically in HSCs.

To further assess the role of *Satb1* in HSC commitment, we modified a recently described method for tracing cell divisions in stem and progenitor cells *in vivo*[25]. Here, we purified donor-derived CD150^{+} LSK cells from long-term reconstituted recipients and labeled them with 5-chloromethylfluorescein diacetate, a cell division tracer. These cells were then transplanted into a second cohort of sublethally irradiated recipients and assessed by monitoring cell division and CD150 expression of the individual donor-derived HSCs (Fig. 4a). We used CD150 as a marker as it has been demonstrated that HSCs downregulate CD150 upon commitment to differentiation[26, 27]. Applying this novel strategy we found that Satb1-deficient CD150^{+} LSK HSCs downregulate CD150 after fewer cell divisions post transplantation in comparison to wild-type HSCs (Fig. 4a,b). After two divisions, $54.3 \pm 15.5\%$ of *Satb1*−/− HSCs versus $81.2 \pm 12.5\%$ of wild-type HSCs still expressed CD150. After three divisions, $28.6 \pm 11.4\%$ of the *Satb1*−/− HSCs vs. $48.8 \pm 7.4\%$ of the wild-type HSCs expressed CD150 (Fig. 4b). These observations indicate that HSC commitment is quantitatively increased in the absence of *Satb1*.

Satb1 regulates the fate of HSC by modulating the division mode

The impairment of long-term repopulation capacity and the increased commitment of *Satb1*−/− HSCs, led us to hypothesize that Satb1 regulates the division mode of HSCs by promoting symmetric self-renewal divisions and repressing differentiation divisions. To test this, we quantified symmetric and asymmetric divisions in individual *Satb1*−/− and wild-type HSCs, utilizing staining for the cell fate determinant and polarity factor *Numb* as previously described[28, 29]. Increased Numb protein expression in one of two daughter cells indicates an asymmetric division, detection of high Numb expression in both daughter cells shows symmetric differentiation divisions, while sustained low levels of Numb in both daughter cells marks symmetric self-renewal divisions (Fig. 4c). We quantified division types of individual HSCs and found a significant, 6.2-fold decrease of symmetric self-renewal divisions in *Satb1*−/− HSCs in comparison to wild-type HSCs ($5.2 \pm 5.4\%$ versus $32.4 \pm 7.2\%$), while symmetric differentiation divisions were significantly increased in *Satb1*−/− HSCs compared to wild-type HSCs ($61.4 \pm 5.5\%$ vs. $35.2 \pm 13.5\%$; Fig. 4d). These observations show that *Satb1* promotes self-renewal and suppresses differentiation commitment of HSCs by regulating the type of stem cell division.

Satb1 regulates Notch targets through repression of *Numb* in HSCs

Regulation of Numb has mainly been reported at the protein level[30, 31], and *Numb* was recently also found to be transcriptionally regulated in *Drosophila* sensory bristle cells[32]. Transcriptional or epigenetic regulation of *Numb* in mammalian stem cells is unknown. We quantified *Numb* mRNA expression in *Satb1*−/− and wild-type CD150^{+} CD48^{−} LSK HSCs and found a two-fold increase of *Numb* mRNA expression in *Satb1*−/− HSCs compared to wild-type HSCs (Fig. 4e). Numb is a negative regulator of Notch signaling, which has been reported to modulate cell-fate decisions of HSC[30, 31]. We therefore assessed whether

elevated *Numb* expression in the absence of *Satb1* has an effect on the transcription of Notch target genes. We found that *Satb1*$^{-/-}$ CD150$^+$ LSK HSCs, as well as highly purified CD150$^+$ CD48$^-$ LSK HSCs, showed significantly reduced levels of Notch targets, including *Hes1* (by 60 ± 13%), *Hes5* (by 82.5 ± 6.6%), *Dtx1* (by 88.5 ± 19.4%) and *Hey1* (by 83.4 ± 9.2%) in comparison to wild-type HSCs (Fig. 4f, Supplementary Fig. 3a,b). To further test whether Numb is downstream of *Satb1* and whether elevated *Numb* expression was functionally critical for the altered cell fate of *Satb1*$^{-/-}$ HSCs we carried out rescue experiments (Fig. 4g,h). Ectopic re-expression of Satb1 in Satb1-deficient HSCs to a level similar to wild-type HSCs led to restoration of *Numb* expression, as well as *Hes1* expression (Fig. 4g, Supplementary Fig. 3c). Moreover, shRNA-mediated knock down of elevated Numb in *Satb1*$^{-/-}$ CD150$^+$ CD48$^-$ LSK HSCs by 60 ± 3.1% lead to a significant reduction of the increased number of colony-initiating cells by reducing CFU-GEMMs (reduced by 58.2 ± 6.7%), CFU-GMs (reduced by 45.8 ± 2%) and BFU-Es (reduced by 30 ± 8%) compared to non-targeting control-transduced cells (Fig. 4h, Supplementary Fig. 3d). Consistent with this observation, the expression of *Hes1*, *Hes5* and *Dtx1* was de-repressed in comparison to non-targeting control-transduced *Satb1*$^{-/-}$ CD150$^+$ CD48$^-$ LSKs (by 2.9 ± 0.2-fold, 2.8 ± 0.4-fold, and 4.3 ± 0.8-fold respectively; Supplementary Fig. 3e). Interestingly, shRNA-mediated knock-down of *Numb* in wild-type HSCs did not cause a significant change in the number of colony-initiating cells (Fig. 4h). These results demonstrate that *Satb1* modulates cell fate determination of HSCs, at least in part, through regulation of *Numb* expression and Notch signaling. The fact that downregulation of *Numb* was sufficient to rescue the increased differentiation commitment of *Sabt1*$^{-/-}$ HSCs but did not have an effect in wild-type HSCs, suggested that additional mechanisms contribute to the changes in cell fate in Satb1-deficient HSCs.

Satb1 deficiency alters transcriptional networks in HSCs

To obtain insight into potential cooperating factors contributing to the increase of differentiation commitment in Satb1-deficient HSCs, we measured gene expression changes in *Satb1*$^{-/-}$ HSCs. Microarray analysis of adult wild-type and *Satb1*$^{-/-}$ HSCs identified 631 differentially expressed genes (Supplementary Table 1) of which 73.3% showed increased and 26.3% showed decreased expression, supporting a role of Satb1 as an overall transcriptional repressor in HSCs. Ingenuity Pathway Analysis (IPA) revealed that *Satb1*-dependent genes in HSCs were highly enriched for gene networks regulating cellular assembly and organization, and cell cycle (Supplementary Fig. 4a). We validated the altered expression of a subset of genes from both categories by real time PCR in an independent set of samples. We confirmed that genes involved in cell cycle activation (*Rbbp9*: 3.5 ± 1-fold, *Kdm3a*: 2.2 ± 0.3-fold, *Chaf1a*: 4.2 ± 1.9-fold and *Bgn*: 36 ± 21.3-fold) and genes regulating cellular organization and contributing to cellular polarity (*Iptr1*: 2.1 ± 0.46-fold, *Tnik*: 2.3 ± 1.7-fold) were significantly overexpressed in *Satb1*$^{-/-}$ HSCs (Supplementary Fig. 4b). These data show that Satb1 regulates different functional gene networks in HSCs, which are supportive of the observed phenotype of enhanced cell cycle activity and differentiation commitment of *Satb1*$^{-/-}$ HSCs.

Gene set enrichment analysis (GSEA)[33] of differentially expressed genes in absence of *Satb1* identified a core set of direct *Myc* target genes[34] positively enriched in the *Satb1*$^{-/-}$

HSCs (normalized enrichment score: 1.90, nominal p-value < 0.001) (Fig. 5a, Supplementary Fig. 4c). Validation by quantitative real-time PCR demonstrated that several *Myc* targets including *Igf1R* (2.9 ± 0.2-fold), *Clasp1* (19.6 ± 13.3-fold), *Tlr4* (1.9 ± 0.2-fold), and *Uhrf2* (1.47 ± 0.2-fold) (Fig. 5b), as well as *Myc* itself (1.66 ± 0.2-fold) were overexpressed in *Satb1*$^{-/-}$ CD150$^+$ CD48$^-$ LSK HSCs compared to wild-type HSCs (Fig. 5c). To assess whether *Myc* is downstream of *Satb1*, as it was previously shown in T cells[21], we measured *Myc* expression in *Satb1*$^{-/-}$ HSCs upon lentiviral re-expression of Satb1. Restoration of Satb1 expression in Satb1-deficient CD150$^+$ CD48$^-$ LSK HSCs led to a normalization of expression of *Myc*, and its target *Igfr1* (Fig. 5d). These data show that Satb1 regulates transcriptional networks involved in cell cycle regulation and cellular organization in HSCs.

Increased *Myc* activity is functionally relevant for enhanced differentiation commitment of Satb1-deficient HSCs

To test whether the *Satb1*-dependent increase of Myc activity is functionally relevant in *Satb1*$^{-/-}$ HSCs, we treated Satb1-deficient CD150$^+$ CD48$^-$ LSK HSCs with two different small molecule Myc inhibitors (10058-F4 and JQ1) and assessed colony-initiating capacity. Both 10058-F4, which has been shown to specifically interfere with Myc transactivation[35], as well as JQ1, a bromodomain/BRD4 inhibitor causing direct repression of *Myc* transcription[36], were found to impair *Myc* target gene expression (Supplementary Fig. 5a,b) and colony formation of Satb1-deficient HSCs (Supplementary Fig. 5c,d) in a dose-dependent manner. We then tested a low effective inhibitor concentration (15μM of 10058-F4 and 250nM of JQ1) on both *Satb1*$^{-/-}$ and wild-type HSCs, and found a reduction of CFU-GEMMs by 39 ± 1.9%; CFU-GMs by 48.9± 8%; and BFU-Es by 45 ± 2.8% for 10058-F4 in comparison to DMSO-treated controls, and a reduction of CFU-GEMMs by 56.8± 1.9%,CFU-GMs by 51± 5.6% and BFU-Es by 47.2± 2.7% by JQ1 in Satb1-deficient HSCs, demonstrating a rescue of the increased number of colony forming units (Fig. 5e,f). We did not observe an effect of inhibitors on wild-type CD150$^+$CD48$^-$LSK HSCs (Fig. 5e,f). These results show that elevated *Myc* activity is functionally important in *Satb1*$^{-/-}$ HSCs. Of note, *Numb* expression was not significantly changed upon Myc inhibitor treatment of *Satb1*$^{-/-}$ HSC (Supplementary Fig. 5e).

Satb1-deficient HSCs display widespread epigenetic changes

We assessed whether Satb1 binds to the *Numb* and *Myc* promoter regions in HSCs by performing chromatin immunoprecipitation (ChIP) using a hematopoietic stem cell line (HPC7)[37]. We found that Satb1 binds to chromatin upstream of the transcriptional start sites of *Numb* and *Myc* (Fig. 6a,b, Supplementary Fig. 6a,b). As Satb1-dependent gene regulation has been linked with epigenetic modifications, such as histone modifications and DNA cytosine methylation[16, 21], we analyzed permissive (H3K4me3) and repressive (H3K27me3) histone marks at the *Numb* and *Myc* promoters. ChIP of primary *Satb1*$^{-/-}$ and wild-type HSCs revealed that absence of Satb1 significantly increased the H3K4me3 mark at both the *Numb* and *Myc* promoter regions (Fig. 6c,d), which is in line with the elevated expression of *Numb* and *Myc* in *Sabt1*$^{-/-}$ HSCs.

We further evaluated genome-wide DNA cytosine methylation by enhanced reduced representation bisulfite sequencing (ERRBS) of DNA extracted from sorted HSCs and MPPs. Comparison of *Satb1*$^{-/-}$ HSCs to wild-type HSCs revealed significant differences in DNA cytosine methylation, with a total of 11,924 differentially methylated regions (DMRs; 1kb genomic tiles, no overlap) comprising 5,089 hypomethylated and 6,835 hypermethylated DMRs (Fig. 6e, Supplementary Table 4). *Satb1*$^{-/-}$ associated DMRs were predominantly located in CpG islands and isolated CpGs, without a strong preference for location within different genomic regions, but with a slight increase in the occurrence of DMRs in intergenic regions (Fig. 6f). Next, we compared wild-type HSCs and wild-type MPPs to define methylation changes associated with normal HSC commitment. We identified a total of 14,778 HSC commitment-associated DMRs (Supplementary Fig. 6c), which were primarily located in CpG islands and isolated CpGs, and without a strong preference for inter- or intragenic regions (Supplementary Fig. 6d). When we compared these normal HSC commitment-associated DMRs with the DMRs identified in Satb1-deficient HSCs, we found a highly significant overlap (p=1.2×10^{-37}; hypergeometrical testing), with 37% shared hypermethylated DMRs and 15% shared hypomethylated DMRs (overall 22% shared DMRs) (Supplementary Fig. 6e).

We further evaluated whether methylation changes were accompanied by gene expression changes in *Satb1*$^{-/-}$ HSCs and found a set of 67 genes showing both significant alterations in gene expression and methylation in the vicinity of the gene (Supplementary Table 5). IPA analysis revealed enrichment of several functionally relevant networks (Supplementary Fig. 6f, Supplementary Table 6). Notably, amongst those was a subset of genes whose differential expression we had previously validated by qRT-PCR (*Itpr1*, *Tnik*) in *Satb1*$^{-/-}$ HSCs, and which have known roles in cell cycle and cellular assembly and organization (Supplementary Fig. 4b)[38, 39]. Taken together, these data show that Satb1 acts as an epigenetic regulator in HSCs by modulating histone marks and DNA cytosine methylation, and indicate that *Satb1* deficiency leads to a commitment-primed epigenetic state in HSCs.

Discussion

The interaction between transcription factor networks is a key mechanism of cell fate decisions in pluripotent hematopoietic cells, including HSCs[40-42]. The biological outcome of simultaneous activity of multiple transcriptional networks depends on the exact cellular and temporal context as HSCs commit and differentiate[70]. However, how transcriptional networks themselves are established and coordinately regulated in stem cells is still largely unknown. Our study identifies the chromatin-remodeling factor *Satb1* as a regulator of transcriptional programs instructing quiescence, self-renewal and commitment in HSCs.

Quiescent HSCs exhibit superior long-term engraftment potential over HSCs in the $G_1/S/G_2/M$ phase[24,43]. The restriction of cell cycling of HSCs prevents their premature depletion and hematopoietic failure under stress conditions[44]. Our study revealed that genes important for cell cycle activation including factors important in the transition from a quiescent (G_0) to an active stage (G_1) were derepressed in *Satb1*$^{-/-}$ HSCs. Consistent with these findings, *Satb1*$^{-/-}$ HSCs were in a more activated state with significantly less HSCs in the G_0 and more in the G_1 phase of the cell cycle in comparison to Satb1-expressing HSCs.

In contrast to the G_0 phase, G_1 is the cell cycle phase in which intrinsic signals can influence cell fate. Integration and interpretation of transcriptional programs determine whether a cell enters S phase or pauses during G_1, until the cell makes the decision whether to self-renew, differentiate or undergo apoptosis[45]. Enhanced progression of *Satb1*^{−/−} HSCs into G_1 may alter their proneness to cell fate specification by making them more susceptible to commitment-inducing factors. Interestingly, *Satb1*^{−/−} HSCs displayed a quantitatively increased generation of committed progenitor cells, indicating that *Satb1* is critical for suppressing HSC commitment and links HSC quiescence with differentiation.

Chromatin-remodeling factors have been found to regulate cell fate in embryonic stem cells[39] and invertebrate stem cells[46]. We found that *Satb1*^{−/−} HSCs undergo significantly more symmetric commitment divisions at the expense of symmetric self-renewal divisions, while the rate of asymmetric divisions remained unchanged. Two Satb1-dependent gene networks were directly involved in the regulation of cellular polarity, differentiation, and proliferation. In *Satb1*^{−/−} HSCs, expression of *Myc* and several of its transcriptional targets, and expression of the negative Notch regulator, *Numb*, was increased. Enforced expression or activation of Myc can lead to an increase in differentiation at the expense of self-renewal in HSCs[47]. Similarly, relatively modest elevation of Numb expression can also induce differentiation of HSCs[29], suggesting that Satb1 inhibits differentiation commitment, at least in part, via the repression of *Myc* and *Numb*. Indeed, independent Numb and Myc rescue experiments showed that the combination of both increased Myc and increased Numb is functionally critical for the increased commitment of *Satb1*^{−/−} HSC.

Numb is a segregating cell fate determinant and tissue-specific repressor of the Notch pathway[30, 31]. Numb-mediated suppression of Notch in HSCs can induce differentiation[29]. We found that Satb1 negatively regulates *Numb* expression in HSCs and that *Satb1* deficiency leads to Numb-mediated inhibition of Notch target gene expression. Impairment of the Notch target genes *Hes1* and *Hes5* in HSCs was demonstrated to cause a loss of HSC and overproduction of myeloid progenitor cells[48], which is consistent with the observed phenotype and the functional rescue experiments in *Satb1*^{−/−} HSCs. Restoration of Satb1 expression in *Satb1*^{−/−} HSCs led to a normalization of elevated *Numb* levels and a significant increase of *Hes1*. Furthermore, restoration of *Numb* expression normalized *Hes1*, *Hes5*, and *Dtx1* expression, and rescued the increased colony-initiating capacity of *Satb1*^{−/−} HSCs. These data show that in the absence of *Satb1*, elevated *Numb* mediates the reduction of symmetrical self-renewal divisions and the concomitant increased production of multipotent progenitor cells, which ultimately depletes the pool of *Satb1*^{−/−} HSCs.

In T cells, Satb1 binds the *Myc* promoter and instructs histone modifications[21]. We found that Satb1 binds both the *Numb* and *Myc* promoters in HPC7 cells, and restoration of Satb1 expression in *Satb1*^{−/−} HSCs rescued elevated *Numb* and *Myc* expression. These observations, together with the finding of increased *Numb* and *Myc* expression in *Satb1*^{−/−} HSCs, show that both *Numb* and *Myc* are downstream of Satb1. It is possible that this regulatory function of Satb1 is indirect and that cofactors are required.

Satb1 acts as an epigenetic regulator and chromatin organizer in T cells and erythroid cells[20] and is accompanied by alterations in histone modifications[16]. Our data show that absence of

Satb1 increases the permissive H3K4me3 mark at both the *Numb* and the *Myc* promoters in *Satb1*^{−/−} HSCs. In addition, we detected significant differences in DNA cytosine methylation in *Satb1*^{−/−} HSCs, which resembles wild-type MPPs and indicates a "commitment-primed" epigenetic state of *Satb1*^{−/−} HSCs. These findings further support our observation of increased differentiation commitment and reduced self-renewal of *Satb1*^{−/−} HSCs, and show that *Satb1* acts as an epigenetic regulator in HSCs by modulating histone marks and DNA cytosine methylation.

Impairment of Satb1 activity is associated with a subset of patients with AML[15]. Moreover, myeloid biased hematopoiesis was recently found in murine loss-of-function models of positive Notch regulators, and loss-of-function mutations of the Notch pathway were identified in patients with chronic myelomonocytic leukemia, consistent with the possibility that myeloid differentiation commitment of HSCs is enhanced by reduced Notch activity[49]. This suggests a possible role of *Satb1* inactivation in stem and progenitor cells in leukemia pathogenesis. As *Satb1* is important for epithelial-mesenchymal transition and elevated Satb1 levels were found in epithelial tumors[17, 50], it will be of interest to determine whether *Satb1*, similar to its function in hematopoietic stem cells, modulates cell polarity and self-renewal in tumor stem cells, and may thereby offer novel opportunities for tumor stem cell-directed therapy.

In summary, our study demonstrates that *Satb1* critically modulates HSC fate decisions by acting as a regulator of multiple, functionally linked HSC properties. Our data show that *Satb1* is crucial for sustained HSC self-renewal, through simultaneously governing gene networks controlling cell fate, promoting quiescence and repressing lineage commitment in HSCs.

ONLINE METHODS

Mice

Satb1^{−/−} mice[12] were kindly provided by Dr. T Kohwi-Shigematsu. C57Bl/6 SJL CD45.1[+] mice were purchased from Jackson Labs (Bar Harbor, ME). All experimental procedures were approved by the Einstein Institutional Animal Care and Use Committee (protocol #2011-0102).

Purification of hematopoietic stem and progenitor cells

Bone marrow cells were isolated from tibiae, femurs and pelvic bones. Fetal liver cells were isolated from E17-18.5 embryos. Red blood cell lysis was followed by negative enrichment using Dynabeads (Invitrogen, Carlsbad, CA) with the following primary antibodies (all PE-Cy5/Tricolor): CD4, CD8a, CD19 (1:100 in PBS/FBS) (eBioscience, San Diego, CA) and B220, Gr-1 (1:50, Invitrogen). Washed, unbound cells were stained with the following antibodies (all 1:30): APC Alexa 750 CD117 (eBioscience), Pacific Blue Sca-1 (Biolegend, San Diego, CA), FITC CD34 (eBioscience), PE-Cy5 CD16/32, PE CD150 (Biolegend), APC CD48 (Biolegend). Cells were sorted using a 5-laser Aria II Special Order System flow cytometer (Becton Dickinson, Franklin Lakes, NJ). Purity of sorted HSCs and MPPs was

>98% for all experiments. Analysis of FACS data was performed using BD FACSDiva (Becton Dickinson) and FlowJo (Tree Star, Ashland, OR) software.

Colony formation and serial replating assays

Fetal liver cells or donor-derived adult stem and progenitor cells were plated in MethoCult M3434 GF+ according to the manufacturer's recommendation (Stem Cell Technologies, Vancouver, BC). Colonies were scored after 7-10 days using an AXIOVERT 200M microscope (Zeiss, Maple Grove, MN).

RNA purification, Real-time PCR, and microarray experiments

RNA was extracted using the RNeasy Micro kit (Qiagen, Valencia, CA), and quantity and quality was assessed using an Agilent 2100 Bioanalyzer (Agilent Technologies, Santa Clara, CA). For real-time RT-PCR, RNA was reverse-transcribed using Superscript II reverse transcriptase (Invitrogen), and amplified using specific primers (Supplementary Table 2) and the universal PCR Power SYBR Green mix (Applied Biosystems, Carlsbad, CA) on an iQ5 real-time PCR detection system (BIO-RAD, Hercules, CA) according to the manufacturer's recommendation. For microarray studies, RNA was amplified using the WT Ovation Pico RNA amplification system (Nugen, San Carlos, CA). After labeling with the GeneChip WT terminal labeling kit (Affymetrix, Santa Clara, CA), labeled cRNA was hybridized to Mouse Gene ST 1.0 microarrays (Affymetrix), stained, and scanned by GeneChip Scanner 3000 7G system (Affymetrix) according to standard protocols.

HSC activation using 5-fluorouracil

4-8 week old Bl/6C57 wild-type mice were injected intra peritoneal (i.p.) with 150 mg/kg 5-fluorouracil (Sigma-Aldrich). After 0-12 days, CD150$^+$ CD48$^-$ LSK and CD150$^+$ CD48$^-$ LSKs were isolated from the pooled bone marrow samples of three injected mice by FACS sorting.

Analysis of microarray data

Raw data was normalized by the RMA algorithm of Affymetrix Power Tools v. 1.178. Significance Analysis for Microarrays within Multiple Experiment Viewer v. 4.8[51], (row average imputation, s0 percentile 5%, delta 0.38742) was combined with raw selection of differentially expressed genes (median expression differences of >1.1-fold). Following removal of unannotated and sex-specific genes varying among the control samples, genes were clustered by hierarchical clustering, with optimization of sample and gene leaf order, using Euclidean distance, complete linkage clustering. Gene Set Enrichment Analysis was performed using all gene sets from mSigDB v3.0 and from the signature database of the Staudt laboratory (http://lymphochip.nih.gov/signaturedb).

Immunohistochemistry

Sorted cells were cytospun on poly-lysine-coated glass slides, dried and fixed with 4% paraformaldehyde, stained, and imaged on a Leica SP5 confocal microscope (Leica, Buffalo Groove, IL). Satb1 and Numb was detected using antibodies against Satb1 (1:250)

(Epitomics, Burlingame, CA) or Numb (1:100) (Abcam, Cambridge, MA) according to the manufacturers' recommendation.

Reconstitution experiments, and competitive serial, and limiting dilution transplantations

1×10^6 nucleated cells from CD45.2$^+$ fetal livers were transplanted into lethally irradiated 6-8 week old C57Bl/6 SJL recipient animals via retro-orbital injection following total body irradiation (950 cGy) using a Shepherd 6810 ^{137}Cs irradiator.

For serial transplantation assays 5×10^5 nucleated CD45.2$^+$ donor cells, 50 CD150$^+$CD11b$^+$Sca-1$^+$Lin$^-$ fetal liver, or adult CD45.2$^+$CD150$^+$ LSK were transplanted along with 5×10^5 CD45.1$^+$ or CD45.1/CD45.2$^+$ total bone marrow competitor cells into lethally irradiated C57Bl/6 SJL mice. After 16-24 weeks, donor cell chimerism and multilineage reconstitution were determined, and CD45.2$^+$ donor cells were isolated from the bone marrow of recipient animals by FACS. 5×10^5 sorted CD45.2$^+$ donor cells were transplanted along with 5×10^5 fresh CD45.1$^+$ or CD45.1/CD45.2$^+$ total bone marrow competitor cells into the next cohort of lethally irradiated C57Bl/6 SJL mice.

Limiting dilution transplantation assays were performed as previously described.[52] Reconstitution was monitored after 8-12 weeks and 16-24 weeks after transplantation. HSCs were quantified as competitive repopulating units using the L-Calc algorithm as previously described.[53]

Analysis of cell cycle activity in HSCs

Cell cycle activity in HSCs was measured using Hoechst 33342 and Pyronin Y incorporation as previously described.[24] Division kinetics of HSCs was determined by culture of sorted, individual, donor-derived wild-type or *Satb1$^{-/-}$* HSCs in CellGro media (CellGenix, Freiburg, Germany) with 50ng/ml mrSCF and 50ng/ml mrTPO. Deposition of individual cells in Terasaki plates was confirmed by microscopy 4hrs after the sort. 48hrs after deposition, the number of wells containing 1, 2 and >2 cells was determined using light microscopy.

HSC division mode assay

To determine symmetric/asymmetric divisions we monitored Numb distribution in HSCs undergoing division by immunohistochemistry as previously described.[29]

Lineage tracing using CMFDA

To monitor HSC commitment kinetics *in vivo*, we modified a previously described protocol for lineage tracing utilizing viability dyes.[25] CD45.2$^+$CD150$^+$ LSK bone marrow cells from > 20 weeks transplanted CD45.1$^+$ mice were labeled with 2μM CellTracker Green CMFDA (Invitrogen). 5000 labeled cells were injected along with 5×10^5 CD45.1$^+$ total bone marrow cells into 6-8 week old 450rad irradiated CD45.1$^+$ mice. 500 labeled HSCs were immediately analyzed for incorporated CMFDA by FACS. Four days after transplantation, recipients were sacrificed, and nucleated bone marrow cells were stained with antibodies against CD45.2, CD150, cKit, Sca-1, and lineage markers. Cells were analyzed using the same flow cytometer set up and experimental protocol as for the initial CMFDA

incorporation analysis. Gates for tracing of up to seven divisions were set as previously described.[54]

Chromatin immunoprecipitation (ChIP)

ChIP experiments were performed as previously described.[28] Chromatin was isolated from murine HPC7 cells and sonicated using a Bioruptor (Diagenode, Denville, NJ). Immunoprecipitation was performed with 5μg Satb1 antibody (Santa Cruz Biotechnology Inc.) or 5μg normal rabbit IgG (Santa Cruz Biotechnology Inc.). Satb1 binding site SBS336 served as a positive control, an intronic IL2 site was used as a negative control.[13] Satb1 binding to the *Myc* promoter was tested using previously published primers.[21]

ChIP on primary cells was performed using the Low Cell# ChIP kit (Diagenode, Denville NJ). CD45+CD150+ LSKs were sorted from the bone marrow of a pool of recipients of *Satb1*−/− or wild-type cells >20 weeks after transplantation. Chromatin was isolated and sonicated using a Bioruptor sonicator. Immunoprecipitation was performed with chromatin from 50,000 sorted cells and 2μg of H3K4me3, H3K27me3 antibodies, or normal rabbit IgG (all from Qiagen). For primers see Supplementary Table S3.

Lentivirus-mediated Satb1 restoration

CD150+CD48− LSKs were isolated from wild-type and *Satb1*−/− embryos at E17-18.5 and infected with lentiviral particles expressing Satb1 or empty vector alone (pCAD-IRES-GFP) in Cellgro medium containing 50ng/ml mrSCF, 50ng/ml mrTPO, and 8μg/ml polybrene (Sigma) as previously described[15]. Viable, GFP+ cells were sorted by FACS (Cell purity >98%, viability >85%).

Numb knock-down

Wild-type or *Satb1*−/− CD45.2+CD150+CD48− LSKs were isolated from recipient mice 16 and 20 weeks after transplantation and transduced with lentiviral shRNAs targeting murine Numb or a non-targeting control (Santa Cruz Biotechnology) by spin infection. Supernatant was replaced with growth medium (Cellgro containing 50ng/ml mrSCF, 50ng/ml mrTPO) after 4hrs and HSCs were cultured for 32hrs. Cells were plated in MethoCult M3434 GF+ containing 1μg/ml puromycin (Sigma). Colonies were scored and mRNA expression was measured 7-10 days after plating.

Myc inhibition

Wild-type and *Satb1*−/− CD45.2+CD150+CD48− LSKs were isolated from recipient mice 16 and 20 weeks after transplantation. Cells were treated with 10058-F4 (Santa Cruz Biotechnology, Santa Cruz, CA), or JQ1 (kindly provided by Dr. J. Bradner) in Cellgro medium containing 50ng/ml mrSCF and 50ng/ml mrTPO for 48hrs. 100× pre-dilutions of each inhibitor were prepared in DMSO and added 1:100 to the culture medium of HSCs. 1% DMSO was added to the mock-treated control cells. After 48hr treatment, cells were plated in MethoCult M3434 GF+. Colonies were scored after 7-10 days.

Enhanced Reduced Representation Bisulfite Sequencing (ERRBS)

ERRBS[55] was performed on sorted, *Satb1*^{−/−} and wild-type CD45.2^{+}CD150^{+} LSKs, and wild-type CD45.2^{+}CD150^{−} LSKs >20 weeks after transplantation. 10ng of DNA was digested with MspI. End repair and ligation of paired end Illumina sequencing adaptors was performed, followed by size selection (150-400bp) using gel extraction (Qiagen), and bisulfite treatment using the EZ DNA Methylation Kit (Zymo Research). PCR amplification using Illumina PCR PE1.0 and 2.0 primers was followed by library product isolation using AMPure XP beads (Agencort). Quality control was performed using quantitation on a Qubit 2.0 fluorometer (Invitrogen) and library visualization using Quant-iT dsDNA HS Assay Kit (Agilent 2100 Bioanalyzer). The amplified libraries were sequenced using a 50bp single end read run on a HiSeq2000 (Illumina). Image capture, analysis, and base calling were performed using CASAVA 1.8 (Illumina). Read alignment at CpGs was performed using FAR software (http://sourceforge.net/projects/theflexibleadap/) for adaptor filtering, bismark[56] for whole genome alignment against the mm9 genome, and methylation level calls were performed on reads with a phred quality score >20 and 10 or 5-fold coverage.

Analysis of ERRBS data

Methylation call files were analyzed using methylKit (v.0.5.3)[57] in R/Bioconductor (v. 2.15.2) using non-overlapping 1kb-sized differentially methylated regions (DMRs) (10× coverage, >10% differential methylation, q<0.001). Differential methylation was assessed between wild-type and *Satb1*^{−/−} CD150^{+} LSKs, and between wild-type CD150^{+} LSKs and wild-type CD150^{−} LSKs. DMRs were annotated using UCSC for CpG islands, CpG shores (2kb up- and downstream from CpG islands), and isolated CpG, as well as RefSeq genes from mm9. Promoters were considered as 5kb upstream of transcription start sites; regions farther than 5kb up- or downstream of RefSeq genes were considered intergenic. Region overlaps were determined using bedtools.[58] Overlap of "commitment DMRs" (between wild-type HSCs and MPPs) and "Satb1^{−/−} HSC DMRs" (between *Satb1*^{−/−} and wild-type HSCs), was determined using bismark methylation calls with a minimum coverage of 5 reads per DMC (q<0.001, >25% differential methylation).

Statistical analysis

Statistical analysis of group comparisons was performed using Student's t-test in Excel, Graph Pad Prism. Statistical enrichment analysis was performed using hypergeometrical testing in R.

Supplementary Material

Refer to Web version on PubMed Central for supplementary material.

Acknowledgements

REFERENCES

1. Till JE, McCulloch EA. A direct measurement of the radiation sensitivity of normal mouse bone marrow cells. Radiat. Res. 1961; 175:145–149. [PubMed: 21268707]

2. BeckerR AJ, McCulloch EA, Till JE. Cytological demonstration of the clonal nature of spleen colonies derived from transplanted mouse marrow cells. Nature. 1963; 197:452–454. [PubMed: 13970094]

3. Spangrude GJ, Heimfeld S, Weissman IL. Purification and characterization of mouse hematopoietic stem cells. Science. 1988; 241:58–62. [PubMed: 2898810]

4. Seita J, Weissman IL. Hematopoietic stem cell: self-renewal versus differentiation. Wiley Interdiscip. Rev. Syst. Biol. Med. 2010; 2:640–653. [PubMed: 20890962]

5. Zeng H, Yucel R, Kosan C, Klein-Hitpass L, Moroy T. Transcription factor Gfi1 regulates self-renewal and engraftment of hematopoietic stem cells. EMBO J. 2004; 23:4116–4125. [PubMed: 15385956]

6. Perry JM, Li L. Self-renewal versus transformation: Fbxw7 deletion leads to stem cell activation and leukemogenesis. Genes Dev. 2008; 22:1107–1109. [PubMed: 18451101]

7. Antonchuk J, Sauvageau G, Humphries RK. HOXB4-induced expansion of adult hematopoietic stem cells ex vivo. Cell. 2002; 109:39–45. [PubMed: 11955445]

8. Chang KC, et al. Interplay between the transcription factor Zif and aPKC regulates neuroblast polarity and self-renewal. Dev. Cell. 2010; 19:778–785. [PubMed: 21074726]

9. Scheel C, et al. Paracrine and autocrine signals induce and maintain mesenchymal and stem cell states in the breast. Cell. 2011; 145:926–940. [PubMed: 21663795]

10. Broske AM, et al. DNA methylation protects hematopoietic stem cell multipotency from myeloerythroid restriction. Nat. Genet. 2009; 41:1207–1215. [PubMed: 19801979]

11. Sun Y, Hu J, Zhou L, Pollard SM, Smith A. Interplay between FGF2 and BMP controls the self-renewal, dormancy and differentiation of rat neural stem cells. J. Cell. Sci. 2011; 124:1867–1877. [PubMed: 21558414]

12. Alvarez JD, et al. The MAR-binding protein SATB1 orchestrates temporal and spatial expression of multiple genes during T-cell development. Genes Dev. 2000; 14:521–535. [PubMed: 10716941]

13. Yasui D, Miyano M, Cai S, Varga-Weisz P, Kohwi-Shigematsu T. SATB1 targets chromatin remodelling to regulate genes over long distances. Nature. 2002; 419:641–645. [PubMed: 12374985]

14. Beyer M, et al. Repression of the genome organizer SATB1 in regulatory T cells is required for suppressive function and inhibition of effector differentiation. Nat. Immunol. 2011; 12:898–907. [PubMed: 21841785]

15. Steidl U, et al. A distal single nucleotide polymorphism alters long-range regulation of the PU.1 gene in acute myeloid leukemia. J. Clin. Invest. 2007; 117:2611–2620. [PubMed: 17694175]

16. Savarese F, et al. Satb1 and Satb2 regulate embryonic stem cell differentiation and Nanog expression. Genes Dev. 2009; 23:2625–2638. [PubMed: 19933152]

17. Han HJ, Russo J, Kohwi Y, Kohwi-Shigematsu T. SATB1 reprogrammes gene expression to promote breast tumour growth and metastasis. Nature. 2008; 452:187–193. [PubMed: 18337816]

18. Lakshminarayana Reddy CN, Vyjayanti VN, Notani D, Galande S, Kotamraju S. Down-regulation of the global regulator SATB1 by statins in COLO205 colon cancer cells. Mol. Med. Report. 2010; 3:857–861.

19. Selinger CI, et al. Loss of special AT-rich binding protein 1 expression is a marker of poor survival in lung cancer. J. Thorac. Oncol. 2011; 6:1179–1189. [PubMed: 21597389]

20. Cai S, Han HJ, Kohwi-Shigematsu T. Tissue-specific nuclear architecture and gene expression regulated by SATB1. Nat. Genet. 2003; 34:42–51. [PubMed: 12692553]

21. Cai S, Lee CC, Kohwi-Shigematsu T. SATB1 packages densely looped, transcriptionally active chromatin for coordinated expression of cytokine genes. Nat. Genet. 2006; 38:1278–1288. [PubMed: 17057718]

22. Challen GA, Boles N, Lin KK, Goodell MA. Mouse hematopoietic stem cell identification and analysis. Cytometry A. 2009; 75:14–24. [PubMed: 19023891]

23. Matsumoto A, et al. P57 is Required for Quiescence and Maintenance of Adult Hematopoietic Stem Cells. Cell. Stem Cell. 2011; 9:262–271. [PubMed: 21885021]

24. Passegue E, Wagers AJ, Giuriato S, Anderson WC, Weissman IL. Global analysis of proliferation and cell cycle gene expression in the regulation of hematopoietic stem and progenitor cell fates. J. Exp. Med. 2005; 202:1599–1611. [PubMed: 16330818]

25. Takizawa H, Regoes RR, Boddupalli CS, Bonhoeffer S, Manz MG. Dynamic variation in cycling of hematopoietic stem cells in steady state and inflammation. J. Exp. Med. 2011; 208:273–284. [PubMed: 21300914]

26. Wilson A, et al. Hematopoietic stem cells reversibly switch from dormancy to self-renewal during homeostasis and repair. Cell. 2008; 135:1118–1129. [PubMed: 19062086]

27. Morita Y, Ema H, Nakauchi H. Heterogeneity and hierarchy within the most primitive hematopoietic stem cell compartment. J. Exp. Med. 2010; 207:1173–1182. [PubMed: 20421392]

28. Kharas MG, et al. Musashi-2 regulates normal hematopoiesis and promotes aggressive myeloid leukemia. Nat. Med. 2010; 16:903–908. [PubMed: 20616797]

29. Wu M, et al. Imaging hematopoietic precursor division in real time. Cell. Stem Cell. 2007; 1:541–554. [PubMed: 18345353]

30. Rhyu MS, Jan LY, Jan YN. Asymmetric distribution of numb protein during division of the sensory organ precursor cell confers distinct fates to daughter cells. Cell. 1994; 76:477–491. [PubMed: 8313469]

31. Spana EP, Doe CQ. Numb antagonizes Notch signaling to specify sibling neuron cell fates. Neuron. 1996; 17:21–26. [PubMed: 8755475]

32. Rebeiz M, Miller SW, Posakony JW. Notch regulates numb: integration of conditional and autonomous cell fate specification. Development. 2011; 138:215–225. [PubMed: 21148185]

33. Subramanian A, et al. Gene set enrichment analysis: a knowledge-based approach for interpreting genome-wide expression profiles. Proc. Natl. Acad. Sci. U. S. A. 2005; 102:15545–15550. [PubMed: 16199517]

34. Zeller KI, et al. Global mapping of c-Myc binding sites and target gene networks in human B cells. Proc. Natl. Acad. Sci. U. S. A. 2006; 103:17834–17839. [PubMed: 17093053]

35. Huang MJ, Cheng YC, Liu CR, Lin S, Liu HE. A small-molecule c-Myc inhibitor, 10058-F4, induces cell-cycle arrest, apoptosis, and myeloid differentiation of human acute myeloid leukemia. Exp. Hematol. 2006; 34:1480–1489. [PubMed: 17046567]

36. Delmore JE, et al. BET bromodomain inhibition as a therapeutic strategy to target c-Myc. Cell. 2011; 146:904–917. [PubMed: 21889194]

37. Pinto do OP, Kolterud A, Carlsson L. Expression of the LIM-homeobox gene LH2 generates immortalized steel factor-dependent multipotent hematopoietic precursors. EMBO J. 1998; 17:5744–5756. [PubMed: 9755174]

38. Mahmoudi T, et al. The kinase TNIK is an essential activator of Wnt target genes. EMBO J. 2009; 28:3329–3340. [PubMed: 19816403]

39. Fazzio TG, Huff JT, Panning B. An RNAi screen of chromatin proteins identifies Tip60-p400 as a regulator of embryonic stem cell identity. Cell. 2008; 134:162–174. [PubMed: 18614019]

40. Miyazaki M, et al. The opposing roles of the transcription factor E2A and its antagonist Id3 that orchestrate and enforce the naive fate of T cells. Nat. Immunol. 2011; 12:992–1001. [PubMed: 21857655]

41. Wontakal SN, et al. A large gene network in immature erythroid cells is controlled by the myeloid and B cell transcriptional regulator PU.1. PLoS Genet. 2011

42. Nerlov C, Graf T. PU.1 induces myeloid lineage commitment in multipotent hematopoietic progenitors. Genes Dev. 1998; 12:2403–2412. [PubMed: 9694804]

43. Orford KW, Scadden DT. Deconstructing stem cell self-renewal: genetic insights into cell-cycle regulation. Nat. Rev. Genet. 2008; 9:115–128. [PubMed: 18202695]

44. Cheng T, et al. Hematopoietic stem cell quiescence maintained by p21cip1/waf1. Science. 2000; 287:1804–1808. [PubMed: 10710306]

45. Massague J. G1 cell-cycle control and cancer. Nature. 2004; 432:298–306. [PubMed: 15549091]

46. Xi R, Xie T. Stem cell self-renewal controlled by chromatin remodeling factors. Science. 2005; 310:1487–1489. [PubMed: 16322456]

47. Reavie L, et al. Regulation of hematopoietic stem cell differentiation by a single ubiquitin ligase-substrate complex. Nat. Immunol. 2010; 11:207–215. [PubMed: 20081848]

48. Santaguida M, et al. JunB protects against myeloid malignancies by limiting hematopoietic stem cell proliferation and differentiation without affecting self-renewal. Cancer. Cell. 2009; 15:341–352. [PubMed: 19345332]

49. Klinakis A, et al. A novel tumour-suppressor function for the Notch pathway in myeloid leukaemia. Nature. 2011; 473:230–233. [PubMed: 21562564]

50. Li QQ, et al. Overexpression and involvement of special AT-rich sequence binding protein 1 in multidrug resistance in human breast carcinoma cells. Cancer. Sci. 2010; 101:80–86. [PubMed: 19860849]

51. Kossenkov AV, Ochs MF. Matrix factorization for recovery of biological processes from microarray data. Methods Enzymol. 2009; 467:59–77. [PubMed: 19897089]

52. Maggio-Price L, Wolf NS, Priestley GV, Pietrzyk ME, Bernstein SE. Evaluation of stem cell reserve using serial bone marrow transplantation and competitive repopulation in a murine model of chronic hemolytic anemia. Exp. Hematol. 1988; 16:653–659. [PubMed: 2900155]

53. Szilvassy SJ, Nicolini FE, Eaves CJ, Miller CL. Quantitation of murine and human hematopoietic stem cells by limiting-dilution analysis in competitively repopulated hosts. Methods Mol. Med. 2002; 63:167–187. [PubMed: 21437808]

54. Lyons AB. Analysing cell division in vivo and in vitro using flow cytometric measurement of CFSE dye dilution. J. Immunol. Methods. 2000; 243:147–154. [PubMed: 10986412]

55. Akalin A, et al. Base-pair resolution DNA methylation sequencing reveals profoundly divergent epigenetic landscapes in acute myeloid leukemia. PLoS Genet. 2012; 8:e1002781. [PubMed: 22737091]

56. Krueger F, Andrews SR. Bismark: a flexible aligner and methylation caller for Bisulfite-Seq applications. Bioinformatics. 2011; 27:1571–1572. [PubMed: 21493656]

57. Akalin A, et al. methylKit: a comprehensive R package for the analysis of genome-wide DNA methylation profiles. Genome Biol. 2012; 13:R87. [PubMed: 23034086]

58. Quinlan AR, Hall IM. BEDTools: a flexible suite of utilities for comparing genomic features. Bioinformatics. 2010; 26:841–842. [PubMed: 20110278]
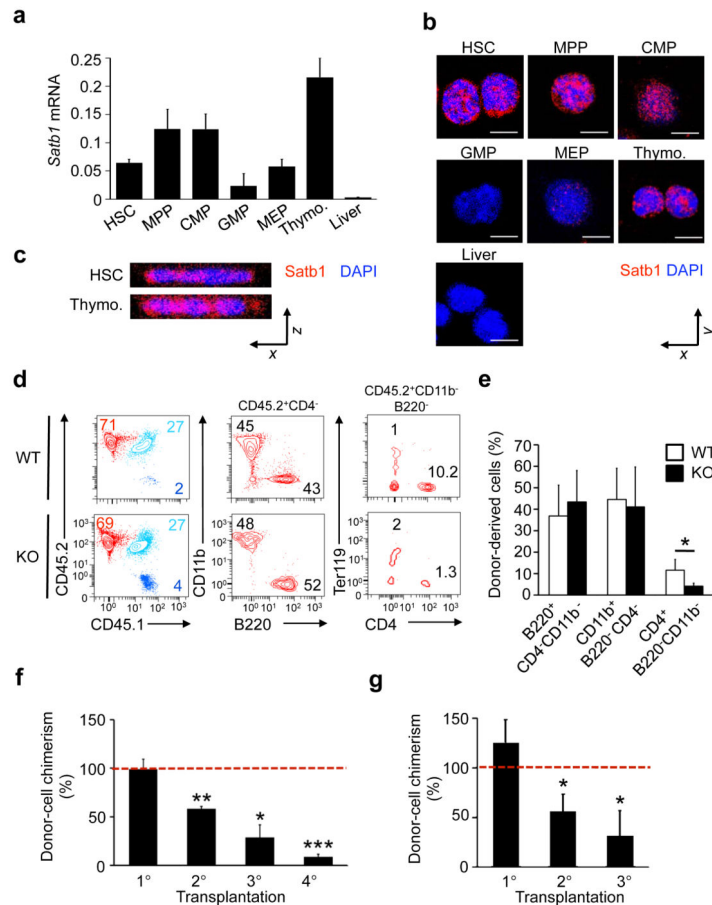
Figure 1. Satb1 is expressed in HSCs and is critical for HSC long-term repopulation capacity
(**a**) Quantitative RT-PCR analysis of *Satb1* mRNA in sorted HSCs, MPPs, CMPs, GMPs, MEPs and thymocytes (Thymo.). Liver cells were used as negative control. Shown are averages and standard deviations of *Gapdh*-normalized expression levels (n=3/population). (**b**) Detection of Satb1 protein by immunohistochemistry and confocal microscopy in HSCs, MPPs, CMPs, GMPs, and MEPs from 6-8 week old Bl6/C57 mice. The nucleus was counterstained with DAPI. Scale bars indicate 5μm. (**c**) Z-stacks of representative images showing nuclear localization of Satb1 in HSCs and thymocytes. (**d**) FACS analysis of multilineage engraftment 16-20 weeks after transplantation of wild-type and *Satb1*$^{-/-}$ HSCs (CD45.2) into recipient mice (CD45.1). Total nucleated cells, donor-derived myeloid cells (CD11b$^+$ CD4$^-$ B220$^-$), B cells (B220$^+$ CD4$^-$ CD11b$^-$) and T cells (CD4$^+$ B220$^-$ CD11b$^-$) are shown. (**e**) Quantification of multilineage engraftment of wild-type and *Satb1*$^{-/-}$ myeloid and lymphoid lineages transferred and analyzed as in **d** (two independent experiments, n=10/genotype, *p<0.05). (**f**) Engraftment of *Satb1*$^{-/-}$ total fetal liver cells in the peripheral blood of serial competitive transplantation recipients (1°, 2°, 3°, 4°) 16-20 weeks after transplantation and expressed as % of the wild-type donor cell engraftment (dashed line) (*p<0.05, **p<0.01, ***p<0.005). (**g**) Engraftment of sorted Satb1$^{-/-}$ CD150$^+$ CD11b$^+$ Sca-1$^+$ Lin$^-$ fetal liver cells in lethally irradiated primary recipients (1°), and of sorted CD150$^+$ LSK HSC in secondary (2°) and tertiary (3°) recipients 20 weeks after

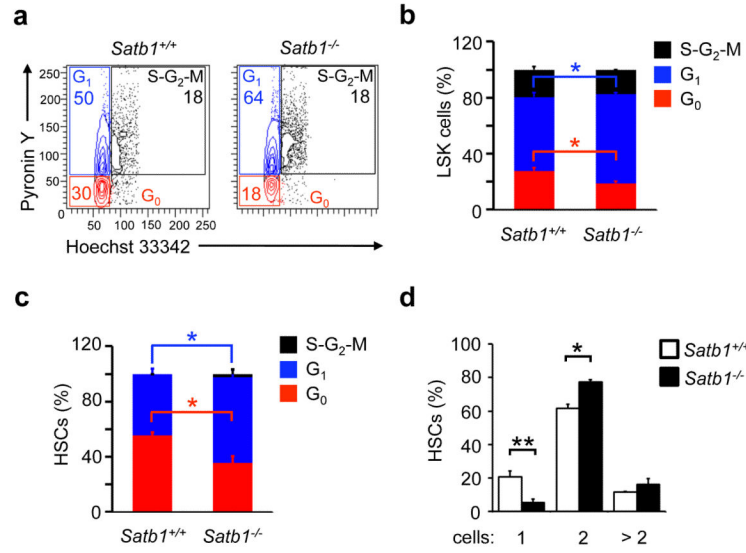transplantation expressed as % of the wild-type donor HSC engraftment (dashed line) (n=12/genotype, *p<0.01).

Figure 2. *Satb1* deficiency leads to reduced HSC quiescence
(**a**) Flow cytometric analysis of cell cycle distribution of wild-type and *Satb1*^{−/−} HSCs 20-24 weeks after transplantation using Pyronin Y and Hoechst 33342 intercalation. Representative FACS plots and gating strategy are shown for LSK cells. (**b**) Quantification of LSK cells in G_0, G_1 and S-G_2-M phases (n=2/genotype, two independent experiments, * p<0.05). (**c**) Quantification of CD150^{+} LSK HSC in G_0, G_1 and S-G_2-M phases (n=2/ genotype, two independent experiments, * p<0.05). (**d**) Division assay of sorted, and individually deposited CD150^{+} CD48^{−} LSK HSCs. Shown are averages and standard deviations of the relative number (%) of wells containing the indicated number of cells after culture of single HSCs (two independent experiments, nTotal=120 cells/genotype; * p<0.05, ** p<0.01).
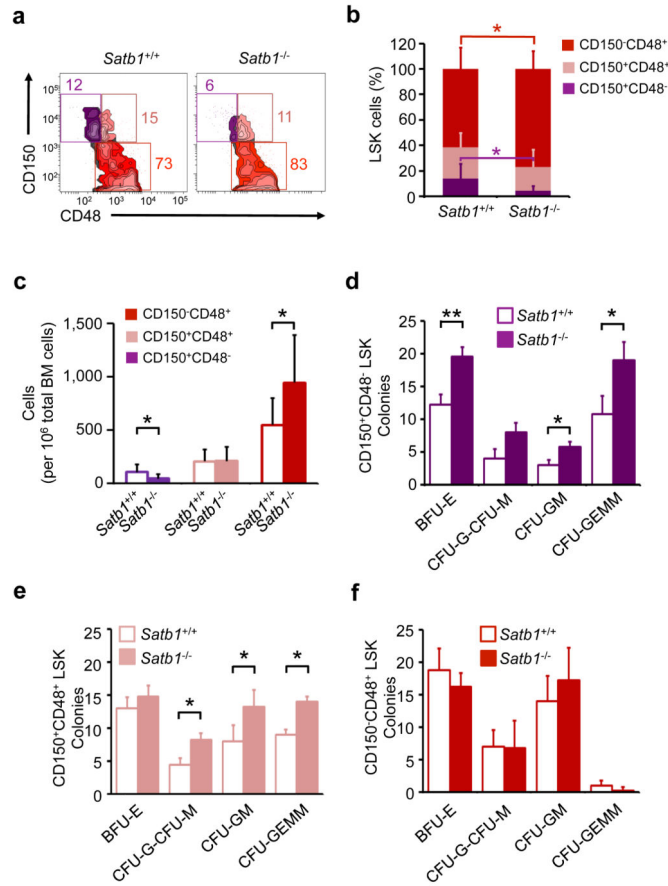
Figure 3. *Satb1* deficiency increases the number of multipotent progenitors and colony-initiating cells originating from the HSC compartment

(**a**) Analysis of phenotypic HSCs and MPPs 20 weeks after transplantation of wild-type or *Satb1*^{−/−} fetal liver cells by FACS. Representative FACS plots analyzing CD45.2^{+} LSK cells gated on CD150^{+} CD48^{−} LSK, CD150^{+} CD48^{+} LSK, and CD150^{−} CD48^{+} LSK cells. (**b**) Quantification of the relative distribution and (**c**) absolute numbers of CD150^{+} CD48^{−} LSK, CD150^{+} CD48^{+} LSK, and CD150^{−} CD48^{+} LSK cells. Shown are averages and standard deviations (n=8/genotype, two independent experiments, * $p<0.05$). (**d**) Colony formation assay of wild-type (open bars) and *Satb1*^{−/−} (solid bars) CD150^{+}CD48^{−} LSK cells. Shown are averages and standard deviations of colony-forming units of the erythroid (BFU-E), granulocytic or monocytic (CFU-G/M), granulocytic-monocytic (CFU-GM), and granulocytic-erythroid-monocytic-megakaryocytic (CFU-GEMM) lineages. (**e**) Colony formation assay of wild-type (open bars) and *Satb1*^{−/−} (solid bars) CD150^{+} CD48^{+} LSK cells. (**f**) Colony formation assay of wild-type (open bars) and *Satb1*^{−/−} (solid bars) CD150^{−} CD48^{+} LSK cells. All assays were plated in M3434 GF+ semisolid medium (n=2/genotype; * $p<0.05$, ** $p<0.01$).
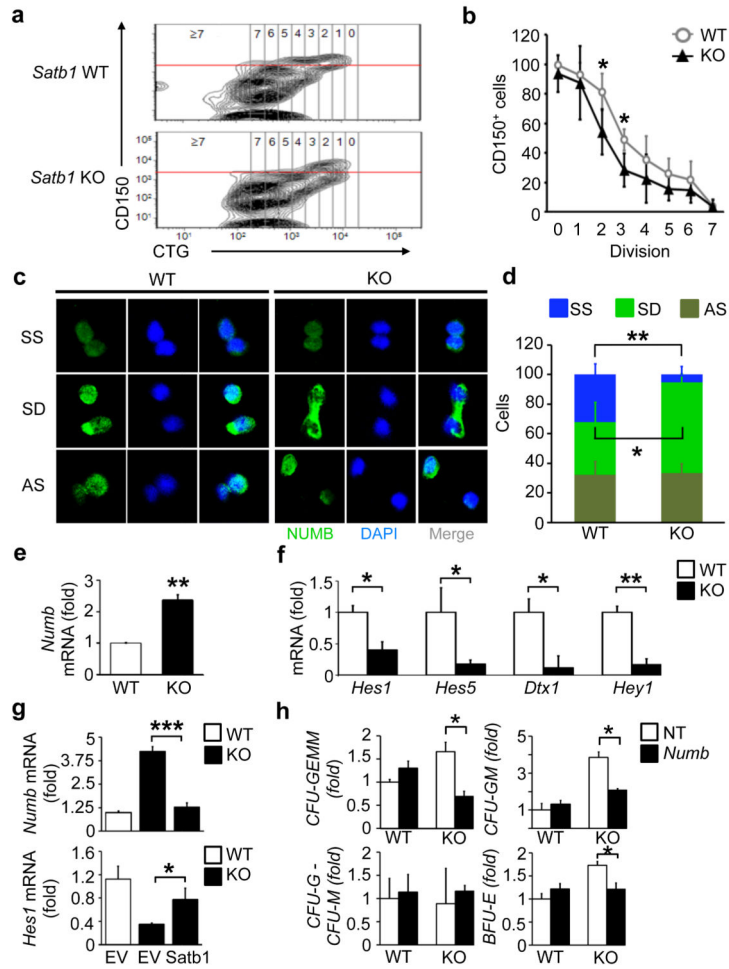
Figure 4. *Satb1*^{−/−} HSCs show increased differentiation commitment, a loss of symmetric self-renewal and an increase in symmetric differentiation divisions

(**a**) *In vivo* commitment tracing of CD150^{+} LSK HSCs using CellTracker Green (CTG). Representative FACS plots showing CTG content and CD150 expression of viable wild-type (WT) and *Satb1*^{−/−} (KO) CD45.2^{+} LSK cells. Horizontal red line indicates analysis cut-off for CD150 expression. Vertical lines separate cells according to their division number. (**b**) Averages and standard deviations of the relative number of CD150^{+} wild-type or *Satb1*^{−/−} CD45.2^{+} LSK cells, expressed as percent of total CD45.2^{+} LSK cells, after 0-7 divisions (n=4/genotype in two independent experiments; * p<0.05). (**c**) Numb staining in individually sorted wild-type and *Satb1*^{−/−} CD150^{+} LSK cells after one division. DNA was counterstained with DAPI. Shown are representative images of symmetric self-renewal (SS), symmetric differentiation (SD), and asymmetric (AS) division. (**d**) Averages and standard deviations of symmetric and asymmetric divisions in wild-type and *Satb1*^{−/−} CD45.2^{+} CD150^{+} LSK cells 24 weeks after transplantation (three independent experiments; wild-type: n=75 cell doublets, *Satb1*^{−/−}: n=85 cell doublets, * p<0.05). (**e**) Quantification of *Numb* mRNA expression in wild-type and *Satb1*^{−/−} CD150^{+} CD48^{−} LSK cells by qRT-PCR. Shown are expression averages and standard deviations normalized to *Gapdh* compared to wild-type HSCs (n=2/genotype, ** p<0.01). (**f**) Quantification of mRNA expression of

Notch target genes *Hes1*, *Hes5*, *Dtx1*, and *Hey1* in wild-type (open bars) and *Satb1*$^{-/-}$ (solid bars) CD150$^+$ LSK cells by qRT-PCR. Shown are averages and standard deviations of the fold change of mRNA expression normalized to *Gapdh* compared to wild-type cells (n=3/ genotype, * p<0.05, ** p<0.01). (**g**) Quantification of *Numb* and *Hes1* mRNA expression by qRT-PCR after lentiviral transduction of wild-type and *Satb1*$^{-/-}$ CD150$^+$ CD48$^-$ LSK cells with either empty vector (EV) or a Satb1-expressing vector (Satb1). Shown are averages and standard deviations normalized to *Gapdh* (* p<0.05, *** p<0.005). (**h**) Colony assay of wild-type and *Satb1*$^{-/-}$ CD150$^+$ CD48$^-$ LSK cells transduced with lentiviral constructs expressing shRNA against *Numb* (*Numb*) or non-targeting shRNA (NT). Shown are averages and standard deviations of the fold change in the number of colony-forming units of the erythroid (BFU-E), granulocytic or monocytic (CFU-G/M), granulocytic-monocytic (CFU-GM), and granulocytic-erythroid-monocytic-megakaryocytic (CFU-GEMM) lineages normalized to the number of lineage-specific colonies generated by NT-treated wild-type HSCs in two independent experiments (n=2/genotype, * p<0.05).
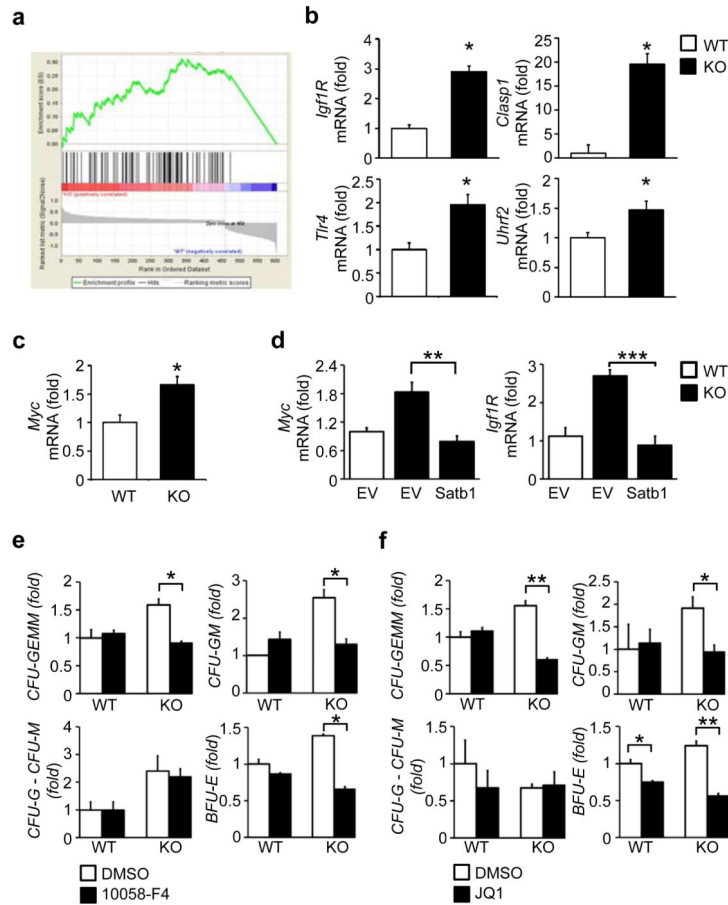
Figure 5. Inhibition of enhanced *Myc* activity restores the increased differentiation commitment of *Satb1*^{−/−} HSCs to wild-type levels

(**a**) Gene set enrichment analysis of the differentially expressed genes in *Satb1*^{−/−} compared to wild-type HSCs showing an enrichment of *Myc* target genes (normalized enrichment score = −1.93, nominal p-value < 0.001). (**b**) Quantification of mRNA expression of Myc targets I*gf1R*, *Clasp1*, *Uhrf2* and *Tlr4* in wild-type and *Satb1*^{−/−} CD150⁺ CD48^{−} LSK cells by qRT-PCR. Shown are expression averages and standard deviations normalized to *Gapdh* compared to wild-type cells (n=3/genotype, * p<0.05). (**c**) Quantification of *Myc* mRNA expression in wild-type and *Satb1*^{−/−} CD150⁺ CD48^{−} LSK cells by qRT-PCR. Shown are expression averages and standard deviations normalized to *Gapdh* compared to wild-type cells (n=3-4/genotype, * p<0.05). (**d**) Quantification of *Myc* and *Igf1R* mRNA expression in wild-type and *Satb1*^{−/−} CD150⁺ CD48^{−} LSK cells after lentiviral transduction with either empty vector (EV) or a Satb1-expressing vector (Satb1) by qRT-PCR. Shown are averages and standard deviations of mRNA expression normalized to *Gapdh* (n=3, ** p<0.01, *** p<0.005). (**e**) Colony assay of wild-type and *Satb1*^{−/−} CD150⁺ CD48^{−} LSK HSCs after 48 hour treatment with 10058-F4, or DMSO. Shown are averages and standard deviations of the number of colony-forming units of the erythroid (BFU-E), granulocytic or monocytic (CFU-G/M), granulocytic-monocytic (CFU-GM), and granulocytic-erythroid-monocytic-megakaryocytic (CFU-GEMM) lineages normalized to the number of lineage-specific colonies generated by DMSO-treated wild-type HSCs. (**f**) Colony assay of wild-type and

Satb1$^{-/-}$ CD150$^+$ CD48$^-$ LSK HSCs after 48 hour treatment with JQ1, or DMSO. Shown are averages and standard deviations of the number of BFU-Es, CFU-G and CFU-Ms, CFU-GMs, CFU-GEMMs normalized to the number of colonies generated by DMSO-treated wild-type HSCs. Data from two independent experiments in technical duplicates are shown (n=2/genotype, * p<0.05, ** p<0.01).
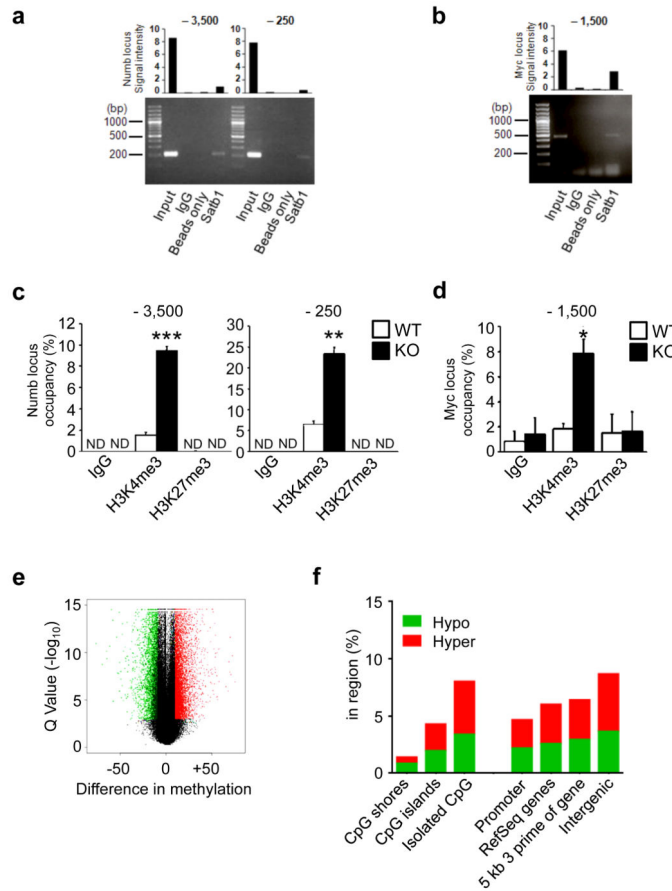
Figure 6. Epigenetic alterations in *Satb1*$^{-/-}$ HSCs

(**a**) Measurement of Satb1 binding to the *Numb* and (**b**) the *Myc* locus by chromatin immunoprecipitation (ChIP) in HPC7 cells. Shown are PCR amplification products of sites at the indicated positions relative to the transcriptional start sites. Bar graphs show the quantification of signal intensities of the PCR products. Normal rabbit IgG antibody and uncoated beads were used as controls. (**c**) Analysis of H3K4me3 and H3K27me3 presence by qChIP in wild-type and *Satb1*$^{-/-}$ CD150$^+$ LSK HSCs at the *Numb* locus. ND: not detectable. (**d**) Analysis of H3K4me3 and H3K27me3 binding by qChIP in wild-type and *Satb1*$^{-/-}$ CD150$^+$ LSK HSCs at the *Myc* locus. Normal rabbit IgG antibody was used as a control. Shown are occupancies of H3K4me3 and H3K27me3 measured in triplicate (pool of n=6/genotype, * p<0.05, ** p<0.01, *** p<0.005). (**e**) Analysis of DNA cytosine methylation in wild-type and *Satb1*$^{-/-}$ CD150$^+$ LSK HSCs by enhanced reduced representation bisulfite sequencing (ERRBS) of (n=2/genotype; two independent experiments). Shown is a volcano plot of a total of 11,924 differentially methylated regions (DMRs) comprising 5,089 hypomethylated and 6,835 hypermethylated DMRs in *Satb1*$^{-/-}$ HSCs compared to wild-type HSCs. (**f**) Relative frequency of hypomethylated (hypo) and hypermethylated (hyper) DMRs with at least 10× coverage as determined by ERRBS within CpG shores, CpG islands, or isolated CpGs, as well as within different genomic features (promoter, RefSeq gene regions, 5kb downstream of RefSeq genes, and in intergenic

regions). Shown are the percentages of DMRs within each region for *Satb1*$^{-/-}$ HSCs compared to wild-type HSCs.